Long non-coding RNA CAR10 promotes angiogenesis of lung adenocarcinoma by mediating nuclear LDHA to epigenetically regulate VEGFA/C

Check for updates

Xiaolu Ge[1,5], Chao Du[2,5], Li Fang[3], Wei Xu[2], Juanjuan Xiang[2], Jiheng Liu[4], Ming Zhou[2], Yuejun Chen[3], Ziyao Wang[2,3] ✉ & Zheng Li ⓘ[2] ✉

Angiogenesis is a significant character of lung adenocarcinoma (LUAD) and is an important reason leading to high mortality rates of LUAD patients. However, the molecular mechanisms of lncRNAs regulating the angiogenesis in LUAD have not been fully elucidated. Here we show lncRNA chromatin-associated RNA 10 (CAR10) was upregulated in the tumor tissue of patients with LUAD and enhanced tumor metastasis. Mechanistically, CAR10 could bind to Lactate Dehydrogenase A (LDHA) protein to regulate the phosphorylation and acetylation of LDHA and increase the dimerization of LDHA to promote its nuclear translocation, which increased the H3K79 methylation in Vascular Endothelial Growth Factor A (VEGFA) and Vascular Endothelial Growth Factor C (VEGFC) gene interval. CAR10 induced microvascular formation in vivo and in vitro by regulating LDHA-VEGFA/C axis. In addition, MYC and TP53 bonded to the promotor of CAR10 and reverse regulated its expression in LUAD cells. CAR10 regulates post-translational modification of LDHA and increases the H3K79 methylation of VEGFA/VEGFC to promote angiogenesis of LUAD, which is a potential therapeutic target for LUAD.

According to *Cancer Statistics, 2023*, lung cancer is the leading cause of cancer-related deaths in women and men worldwide[1]. In China, lung cancer ranks first in terms of both incidence and mortality[2]. Lung adenocarcinoma (LUAD) is the most common subtype according to histological characteristics, accounting for more than half of all lung cancers[3]. With the advancement of tumor molecular biology research, molecular targeted therapy and immunotherapy have gradually been discovered and applied in the treatment of LUAD[4–7]. However, the 5-year overall survival (OS) rate of patients with lung cancer remains only 10%–20% in most countries[8]. Therefore, it is necessary to further understand the key mechanisms driving LUAD development and identify more targets for treatment.

Angiogenesis maintains sufficient blood supply and new blood vessels for the growth and metastases of tumors, including LUAD[9]. Metabolism, one of the hallmarks of cancer, is associated with tumor angiogenesis and metastasis in a wide variety of tumor[10,11]. LncRNAs are important molecules that regulate several cell processes, and dysregulation of lncRNAs contributes to the development of lung cancer through various mechanisms, including angiogenesis[12–14]. LINC00173.v1 promotes angiogenesis by sponging miR-511-5p to promote the progression of lung squamous cell carcinoma[15]. LincRNA-p21 impacts prognosis in resected non-small cell lung cancer patients through angiogenesis regulation[16]. However, the detailed molecular mechanisms of lncRNA participating in the regulation of metabolism and angiogenesis in LUAD remain to be elucidated.

LncRNA chromatin-associated RNA 10 (CAR10) is located on chromosome 10, 10q26.2, and transcript length is 2356 bp[17]. Our previous study found that CAR10 promotes LUAD metastasis via inducing epithelial-to-mesenchymal transition (EMT)[18]. Interestingly, we found that knockout CAR10 decreased the density of blood vessels in xenograft models, suggesting that CAR10 may regulate tumor vasculature formation. In this study, we explore the function and molecular mechanisms of CAR10 inducing angiogenesis in LUAD. CAR10 enhances VEGFA/C expression

[1]Shanghai Key Laboratory of Pancreatic Disease, Shanghai General Hospital, Shanghai Jiaotong University, Shanghai, PR China. [2]The First Department of Thoracic Surgery, Hunan Cancer Hospital and the affiliated Cancer Hospital of Xiangya School of Medicine, Central South University, Changsha, PR China. [3]NHC Key Laboratory of Carcinogenesis, Xiangya School of Basic Medical Sciences, Central South University, Changsha, Hunan, PR China. [4]Department of Hematology & Oncology, First Hospital of Changsha, Changsha, Hunan, PR China. [5]These authors contributed equally: Xiaolu Ge, Chao Du. ✉e-mail: wangziyao@hnca.org.cn; lizheng@csu.edu.cn

and promotes angiogenesis via LDHA in LUAD cells. Mechanically, CAR10 binds to LDHA and regulates the post-translational modifications and nuclear location of LDHA. CAR10 mediates VEGFA/C epigenetic modification through enhancing the interaction between nuclear LDHA and DOT1L. Meanwhile, MYC and TP53 variously regulated the expression of CAR10 in LUAD cells.

Results

CAR10 induces angiogenesis by overexpressing VEGFA/C

We examined the expression of CAR10 in 4 paired LUAD samples with metastasis tissues. CAR10 was found to be overexpressed in LUAD with higher expression in metastatic tissues (Fig. 1A). To investigate the potential role of CAR10 in LUAD metastasis, we performed several analysis methods
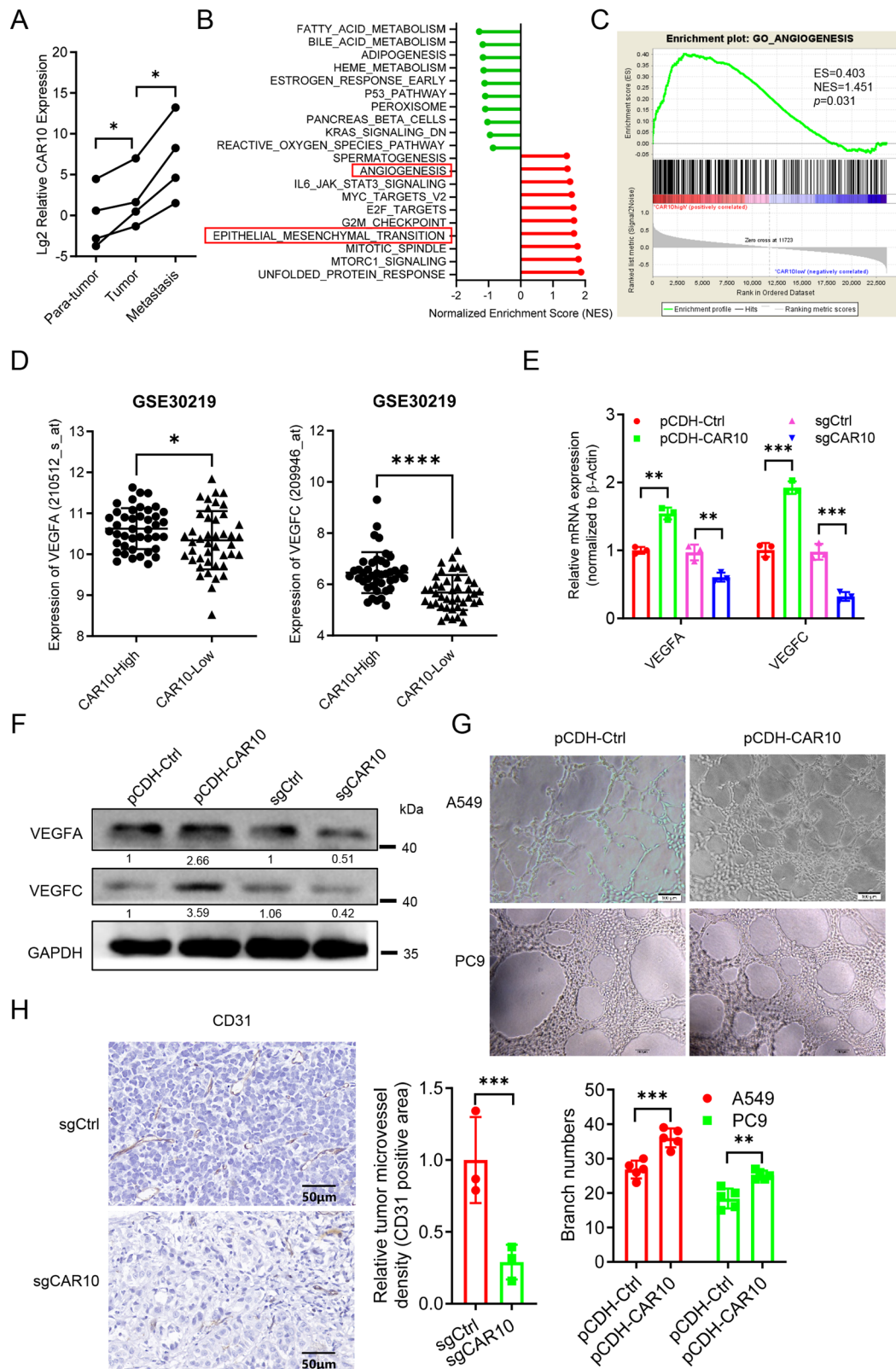
Fig. 1 | CAR10 induces angiogenesis by overexpressing VEGFA/C. A CAR10 expression was analyzed by qRT-PCR in para-tumor (n = 4), matched tumor (n = 4), and metastatic tissue samples (n = 4). All data are presented as the mean ± SEM of three independent experiments, where appropriate, and were analyzed using pair two-tailed Student's *t*-test. **B** GESA analysis of GSE30219 according to the expression of CAR10. NES, normalized enrichment score. The top 10 upregulated and downregulated pathways are shown. **C** GSEA analysis showing that angiogenesis signaling was enriched among the upregulated pathways. ES, enrichment score; NES, normalized enrichment score; *p, p* value. **D** VEGFA and VEGFC expression were upregulated in CAR10-High LUAD tissues in GSE30219 dataset. Data are presented as the mean ± SD, two-tailed Student's *t*-test. **E** Expression of VEGFA and VEGFC mRNA was detected in stably CAR10 overexpressing or knockdown A549 cells. Data are presented as the mean ± SEM of three independent experiments, two-

tailed Student's *t*-test. **F** Western blot analysis of the VEGFA and VEGFC proteins expression in stably CAR10 overexpressing or knockdown A549 cells. **G** HUVEC cells were treated with culture supernatant collected from stably CAR10 overexpressing A549 and PC9 cells and followed by detecting with endothelial tube formation. Endothelial tube formation, number of tubes was shown as mean ± SEM; n = 5 independent experiments, two-tailed Student's *t*-test. Scale bar: 100 μm. **H** CD31 expression in tumors subcutaneously xenografted in nude mice was detected by immunohistochemistry. The areas of blood vessels in tumors subcutaneously xenografted are counted. Scale bar: 50 μm. Relative areas of blood vessels were shown as mean ± SEM; n = 3 independent experiments, two-tailed Student's *t*-test. *p < 0.05, **p < 0.01, and ***p < 0.001, NS: no statistical significance.

to analyze the clinic data from GSE30219[19]. Clustering of 242 differentially expressed genes (*P* < 0.05, |log2foldchange| > 1) showed that the majority of differentially expressed genes were significantly upregulated upon CAR10-High expression LUAD tissue (Fig. S1A). GSEA analysis of GSE30219 dataset showed that genes related to EPITHELIAL MESENCHYMAL TRANSITION and ANGIOGENESIS were significantly enriched in the CAR10-High expression group (Figs. 1B, C and S1B). EMT and angiogenesis is an important process in tumor tissue growth and metastasis[20]. Our previous studies demonstrated that CAR10 promotes LUAD metastasis via the miR-203/30/SNAI axis to induce EMT of LUAD cells[18]. Nearly four decades ago, vascular endothelial growth factor (VEGF) was identified as a critical factor promoting vascular permeability and angiogenesis, followed by identification of VEGF family ligands and their receptors (VEGFR)[21,22]. The VEGF family ligands include VEGFA, VEGFB, VEGFC, and VEGFD. Expression correlational analysis of GSE30219 dataset showed CAR10 was positively correlated with the expression of VEGFA and VEGFC, except VEGFB and VEGFD (Figs. 1D and S1C). This observation triggered us to speculate that CAR10 possibly plays an important role in angiogenesis of LUAD via regulating the expression of VEGFA and VEGFC. Furthermore, with CAR10 upregulation in A549 and PC9 cells, we found a corresponding increase in the expression of VEGFA and VEGFC (Figs. 1E, F and S1D, E). Knocking out CAR10 reduced the expression of VEGFA and VEGFC in A549 cells (Fig. 1E, F). The conditioned medium of A549 and PC9 cells with overexpression of CAR10 was collected to culture human umbilical vein endothelial cells (HUVECs). The results showed that the conditioned medium from CAR10 overexpression A549 PC9 cells promoted the tube formation of HUVECs (Fig. 1G). We collected tissues from A549 xenografts in nude mice to perform immunohistochemistry (IHC) and determined the density of blood vessels in tumor. Interestingly, the results showed that the density of blood vessels in the KO-CAR10 (sgCAR10) group was significantly lower than the control group (sgCtrl) (Fig. 1H). These results suggest that CAR10 may regulate angiogenesis via VEGFA/C in LUAD.

CAR10 directly interacts with LDHA in cytoplasm and nucleus

In our results, CAR10 was not interacted with VEGFA or VEGFC through RNA pull-down and WB detection (Fig. S2A). This suggested CAR10 controlled the expression of VEGFA or VEGFC via transcriptional control or epigenetic regulation. For further exploring the mechanism by which CAR10 affects angiogenesis in LUAD, three RNA pull-down experiments combined with an LC-MS/MS analysis were performed to precisely identify proteins that bind to CAR10. Glucose metabolism can regulate cancer metastasis, recurrence, and therapy through participating in signaling transduction or epigenetic regulation related to angiogenesis[23–27]. Fourteen proteins shared in three tests were identified, including four proteins enriched in the metabolism and energy pathways (Fig. S2B–E, Table S2). Followlingly, RNA pull-down and WB results show that LDHA specifically binds to CAR10, rather than G6PD, GPI, or MDH2 (Figs. 2A and S2F). A549 cells were transfected with a vector expressing Flag-tagged LDHA, and then the RIP assay was performed. The results showed that compared with the IgG group, the anti-Flag antibody enriched more CAR10 (Fig. 2B). In addition, we constructed a vector containing a 12 × MS2 binding site with

CAR10 and a vector coding a fused protein Flag-GFP-MS2 binding to MS2 loop RNA, and the MS2-TRAP assay revealed that LDHA specifically binds to CAR10 (Fig. 2C). LDHA protein could be described as having three parts, N terminal domain, NADH-binding domain, and pyruvate-binding domain (Fig. S3A). To confirm the exact binding domains of CAR10 and LDHA protein, we designed different plasmids with missing different structures(Fig. S3A, B). Our MS2-Trap experiments demonstrated that deletion of the first NADH-binding domain and the second pyruvate-binding domain of LDHA abolished or reduced the interactions between LDHA and CAR10 (Fig. 2D). On the other hand, LDHA bound to full-length CAR10, CAR10-M1 and CAR10-M2, but not CAR10-M3 (Fig. 2E). These data suggest that LDHA binds to CAR10 within the region corresponding to RNA sequence 1788–2375, and the first NADH-binding domain and the second pyruvate-binding domain of LDHA were necessary for the interactions between LDHA and CAR10. Using FISH with immunofluorescence (IF) analyses, we verified that CAR10 co-localized with LDHA in cytoplasm and nucleus of A549 cells (Fig. 2F). Our findings support that CAR10 directly interacts with the LDHA protein in cytoplasm and nucleus.

CAR10 promotes angiogenesis and increases VEGFA/C expression via LDHA

To verify that the regulation of angiogenesis by CAR10 depends on LDHA, we designed a series of rescue experiments. The conditioned medium of A549 cells with changing the expression of CAR10 and LDHA was collected to HUVECs. The results showed that the conditioned medium from CAR10 overexpression A549 cells promoted the proliferation of HUVECs, which was blocked by silencing LDHA (Fig. 3A). In contrast, the conditioned medium from CAR10 KO A549 cells decreased the proliferation of HUVECs, while LDHA overexpressing reversed this effect (Fig. 3B). Transwell experiments suggested that knockdown of LDHA could partially reverse the effect of the conditioned medium from CAR10 overexpression A549 cells to enhance the invasion of HUVECs, and vice versa. (Fig. 3C, D, up). Furthermore, we inoculated HUVECs on the surface of matrigel and observed the tubes formation of HUVECs cultured in conditioned medium from A549 cells. The results showed that CAR10 partially regulated tube formation of HUVECs depending on LDHA (Fig. 3C, D, down).

Furthermore, we detected mRNA expression and secreted level of VEGFA and VEGFC in LUAD cells. We found that knockdown of LDHA partially inhibited the intracellular mRNA expression and extracellular exocrine of VEGFA and VEGFC induced by overexpression of CAR10, whereas increasing LDHA expression effectively reversed the inhibition effect induced by CAR10 (Fig. S4A–D). Together, these results suggest that LDHA is required for CAR10 enhancing VEGFA/C expression and promoting tumor vascularization.

CAR10 mediates VEGFA/C epigenetic modification through regulating LDHA post-translational modification and polymerization formation

The expression of LDHA mRNA did not change when CAR10 was overexpressed or knocked down (Figs. 4A and S4B, D). However, the levels of
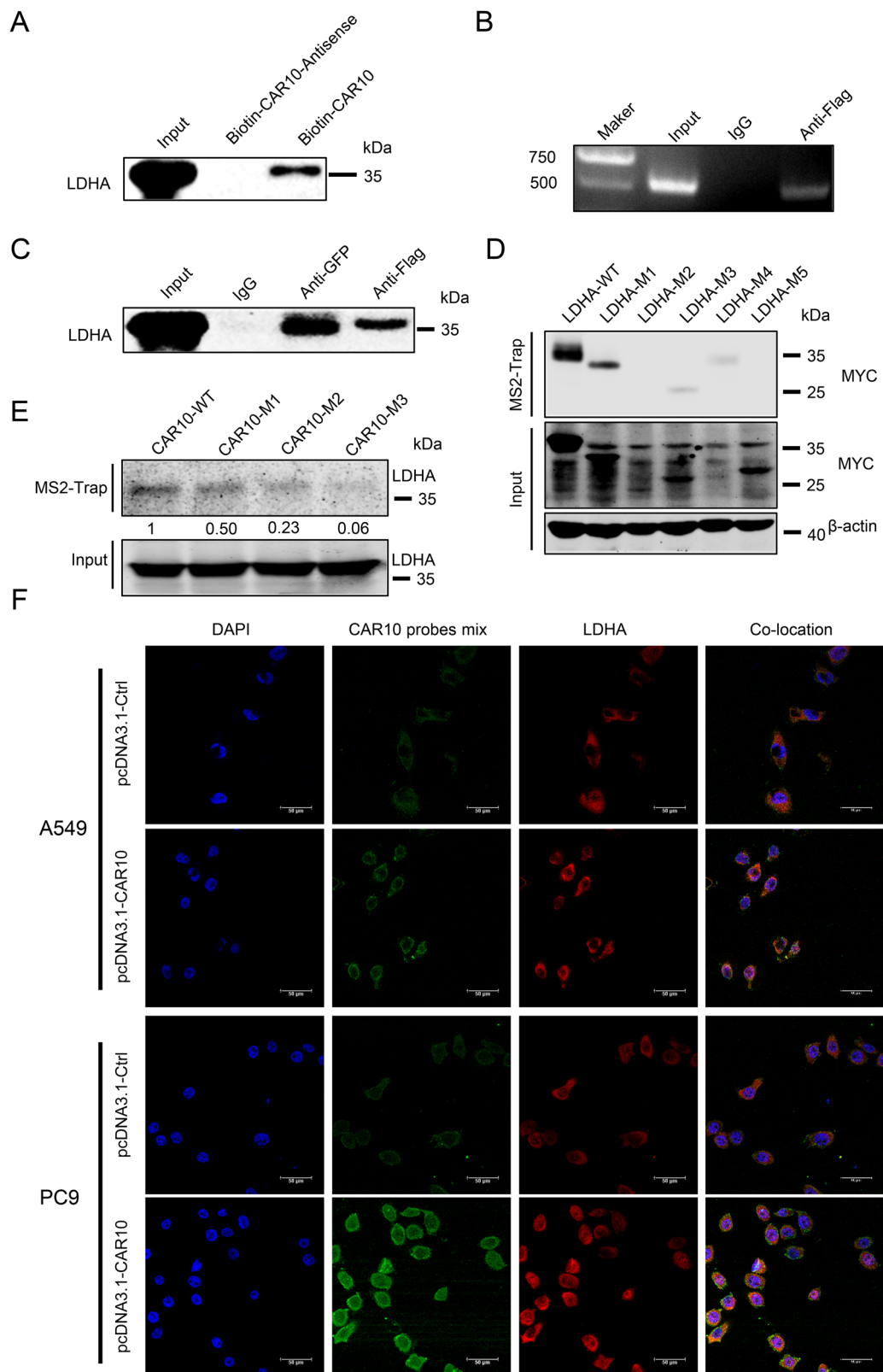
LDHA protein displayed an upward or downward trend when CAR10 was overexpressed or knocked down, respectively, in A549 and PC9 cells (Figs. 4B and S4E). It has been reported that LDHA are able to dimerize and enter the nucleus to exert non-classical enzymatic activity[28]. The results of FISH and IF experiments showed that CAR10 increased the expression of nuclear LDHA (Fig. 2G). We also examined LDHA cytoplasmic and nuclear distribution and found CAR10 promoted the nuclear translocation of LDHA protein (Figs. 4C and S4E). After cross-linked the protein lysate with glutaraldehyde, we found overexpression of CAR10 increased the tetramers, dimers, and monomers of LDHA (Figs. 4D and S4F). According to the recent publications, the enzymatic activity of LDHA is modulated by post-translational modifications, including acetylation and phosphorylation[29,30].

Fig. 2 | CAR10 directly interacts with LDHA in cytoplasm and nucleus. A Western blot analysis of LDHA in RNA pull-down precipitates retrieved by biotinylated CAR10 or biotinylated antisense CAR10 from the lysates of A549. **B** RNA immunoprecipitation experiment in A549 cells transfected with Flag-LDHA fusion expression vector, followed by detecting CAR10 using PCR. **C** MS2-tagged RNA affinity purification experiment in A549 cells transfected with a vector containing 12 × MS2 and CAR10 to form a fusion expression and a vector expressing Flag-GFP-MS2 fusion protein, followed by blotting with LDHA. **D** Human embryonic kidney (HEK) 293T cells stable expressing Flag-GFP-MS2 fusion protein were transfected with plasmids encoding wild-type (WT) CAR10 with 12 × MS2 tag and MYC-tagged wild-type LDHA and mutations 1–5 of LDHA. CAR10-MS2 immunoprecipitates from the transfected cells were immunoblotted with antibodies against MYC tag and β-actin. **E** Human embryonic kidney (HEK) 293T cells stable expressing Flag-GFP-MS2 fusion protein were transfected with plasmids encoding 12 × MS2-tagged wild-type CAR10 and mutations 1–3 of CAR10. CAR10-MS2 immunoprecipitates from the transfected cells were immunoblotted with antibodies against LDHA.
F Localization of CAR10 and LDHA in A549 and PC9 cells analyzed by FISH and immunofluorescence, imaged by confocal microscopy, and merged with DAPI. Scale bar: 50 μm.

Next, we performed immunoprecipitation experiments to detect post-translational modifications of LDHA in A549 cells with overexpressing CRA10. The results displayed that overexpression of CAR10 promoted the phosphorylation of LDHA, especially that of its Y10 phosphorylation, and inhibited LDHA acetylation (Fig. 4E). HER2 and Src are the dominant phosphokinases that phosphorylate LDHA at tyrosine 10[31]. As the reports in literature, our co-immunoprecipitation (IP) experiments demonstrated overexpression of CAR10 enhanced the interaction between LDHA and HER2/SRC, while CAR10 knockdown decreased their interaction (Fig. S4G). These results suggested that CAR10 regulates the balance of phosphorylation and acetylation of LDHA protein to enhance its expression.

DOT1L is the only known enzyme to possess histone methyltransferase activity toward histone H3K79[32]. The hypermethylation of H3K79 is enriched in the gene body and coupled with gene transcription[33]. Nuclear LDHA protein helps DOT1L upregulate the hypermethylation of H3K79, thereby enhancing downstream genes expression[28]. The results of LDHA cytoplasmic and nuclear distribution showed that CAR10 promoted LDHA nuclear translocation. These observations prompted us to speculate that CAR10 increases the hypermethylation of H3K79 in VEGFA/C gene body via increasing LDHA nuclear translocation to enhance the interaction between LDHA and DOT1L. We analyzed the A549 H3K79me2/H3K79me3 chromatin immunoprecipitation (ChIP)-seq data from the ENCODE database, which showed H3K79me2/H3K79me3 modification in the VEGFA and VEGFC gene (Fig. S5A). Subsequently, we performed ChIP-PCR assay using antibodies of H3K79me1, H3K79me2, or H3K79me3 and found obvious H3K79 modifications in the VEGFA/VEGFC gene interval (Fig. S5B, C). Additionally, CAR10 increased the H3K79me3 modification in A549 and PC9 cells (Fig. S5D). We found that LDHA directly bonded to DOT1L in A549 cells (Fig. S5E). Overexpression of CAR10 enhanced the interaction between LDHA and DOT1L, while CAR10 knockdown decreased their interaction (Fig. 4F). ChIP-qPCR assay using antibodies of H3K79me1, H3K79me2, or H3K79me3 and found CAR10 increased the hypermethylation of H3K79 in the VEGFA/VEGFC gene interval (Figs. 4G and S5F). Overall, CAR10 regulating the post-translational modification of LDHA, together with its tetramer-to-dimer transition, increased LDHA protein expression and nuclear location and promoted the extracellular and intracellular expression of VEGFA/C by enhancing the interaction between LDHA and DOT1L to induce the methylation of H3K79 in VEGFA/C gene interval.

CAR10 promotes LUAD development via LDHA-VEGFA/C axis

To examine the effect of CAR10-LDHA-VEGFA/C in tumor angiogenesis, CAR10 overexpression with vector, CAR10 KO, and LDHA overexpression rescue cells were injected subcutaneously into NOD-SCID mice. The results showed the growth of xenograft was significantly increased by over-expressing CAR10 (Fig. 5A). Oppositely inhibited tumor growth was observed upon CAR10 depletion, while LDHA overexpressing reversed the inhibition of tumor growth (Fig. 5B). And IHC analysis showed more tumor microvessel formation and a higher expression of LDHA, VEGFA and VEGFC in CAR10 overexpressing tumors (Fig. 5C, left). On the contrary, less tumor microvessel formation and a lower expression of LDHA, VEGFA, and VEGFC were shown in CAR10 KO tumors, and LDHA overexpressing reversed the tumor microvessel formation and the expression of VEGFA and VEGFC (Fig. 5C, right). CD31 positive tumor microvessel and IHC score of LDHA, VEGFA, and VEGFC had been counted (Fig. 5D). These results further provide evidence that CAR10/LDHA/VEGF was involved in LUAD angiogenesis and development.

We used the combination of CAR10 and LDHA or VEGFA/C as indicators for the prognostic analysis of LUAD in GSE30219. The results suggested that patients with high expression of both CAR10 and LDHA/VEGFA/VEGFC tended to have the worst prognosis compared to the other groups (Fig. S6).

MYC and TP53 competitively regulated the expression of CAR10 in LUAD cells

To investigate the mechanism of high expression of CAR10 in LUAD cells, we screened potential transcription factors of CAR10 using the PROMO and JASPAR programs. We found that TP53 and MYC can bind to the CAR10 promoter region (-2000 to +100), while TP53 binds to the promoter region at −1840 to −1823 and MYC binds to the promoter region at −816 to −807 (Fig. 6A). The ChIP by an anti-TP53/anti-MYC antibody demonstrated the occupancy of TP53/MYC on the CAR10 promoter region (Fig. 6B). qRT-PCR results showed MYC promoted the expression of CAR10, and TP53 inhibited the expression of CAR10 (Fig. 6C). The luciferase reporter assay also showed that MYC strongly increased the luciferase activity of the CAR10 promoter region, while TP53 inhibited the luciferase activity (Fig. 6D, E). All up, these findings show that MYC and TP53 competitively regulated the transcription expression of CAR10 in LUAD.

Discussion

Metastasis is marked as the high malignancy of LUAD and the leading cause of cancer-related deaths[34,35]. Angiogenesis and EMT are closely associated with the process of metastasis in LUAD[36–38]. Our previous studies demonstrated that CAR10 promotes LUAD metastasis via the miR-203/30/SNAI axis[18]. In this study, we found that lncRNA CAR10 promoted the angiogenesis of LUAD by binding LDHA and increasing their nuclear translocation to enhance the hypermethylation of H3K79 in VEGFA/C gene interval. Hence, CAR10 would regulate the growth and metastases of LUAD in various respects. On the other hand, other functions of CAR10 participating in the process of LUAD are unclear.

Angiogenesis as a hallmark of cancer is an extremely complex cascade reaction that is affected by various cell signaling pathways mediated by multiple cytokines and receptors[11]. Lymphangiogenesis and lymph node (LN) metastasis are also thought to participate in cancer metastasis and are associated with patient's poor prognosis[39,40]. The VEGF family and its receptors activate a variety of signaling pathways to play an important role in tumor angiogenesis[41,42]. Some reports have found that lncRNAs are also involved in regulating the expression of VEGF and affecting tumor angiogenesis[43,44]. In this study, in vitro and in vivo experiments showed that CAR10 promoted angiogenesis via increasing the expression of VEGFA and VEGFC. VEGFA induces proliferation and migration of vascular endothelial cells and mainly participates in both physiological and pathological angiogenesis[45]. VEGFC can bind and activate VEGFR-2 and VEGFR-3
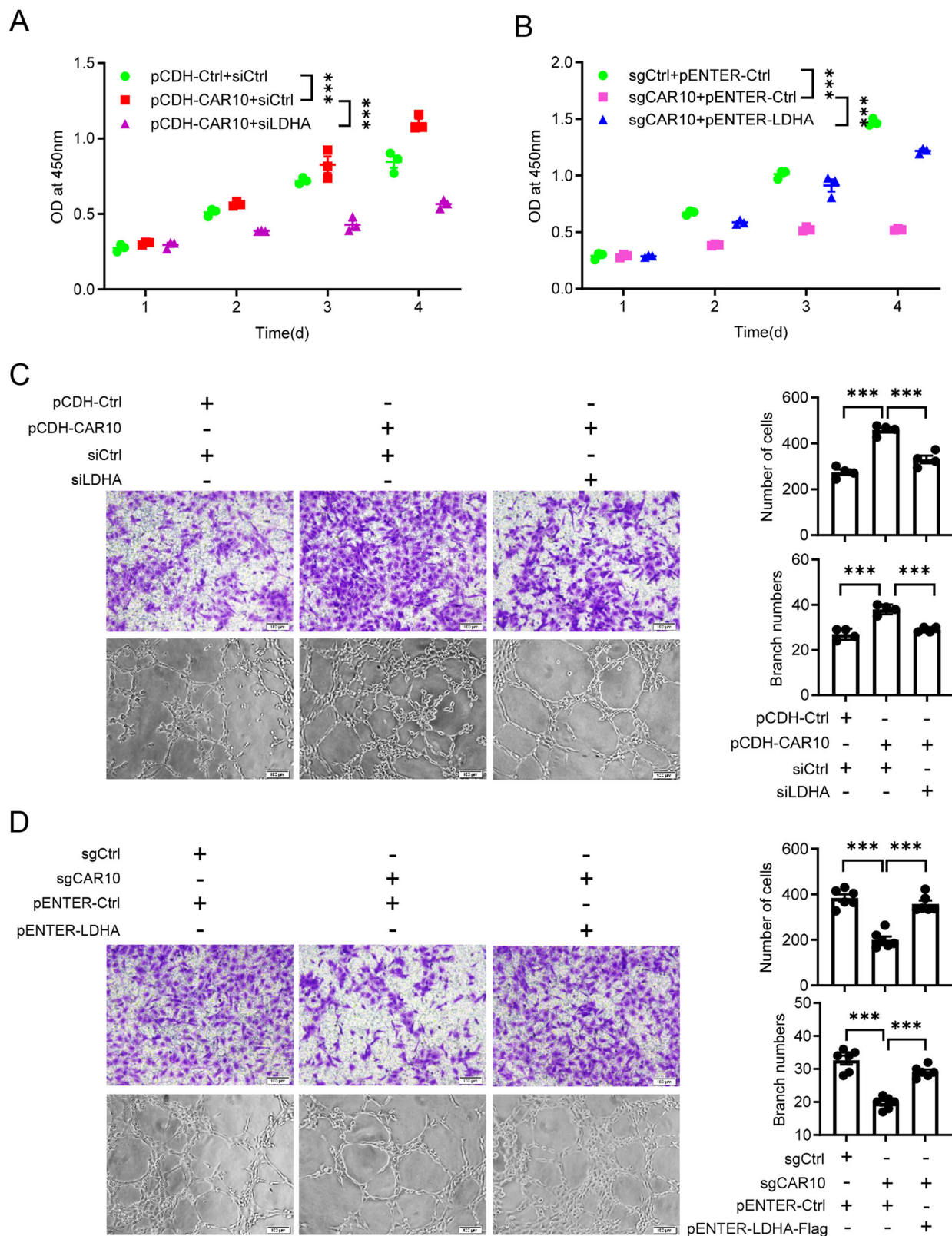
Fig. 3 | CAR10 promotes angiogenesis via LDHA. A HUVEC cells were treated with culture supernatant collected from stably CAR10 overexpressing or knockdown A549 cells transfected with siLDHA or pENTER-LDHA and followed by detecting with cell counting Kit 8 (CCK8) (**A**, **B**), Matrigel Invasion Assay (**C**) and endothelial tube formation (**D**). CCK8, $n = 3$, non-parametric Mann–Whitney test. Matrigel Invasion Assay, number of invasive cells was shown as mean ± SEM; $n = 3$ independent experiments, two-tailed Student's t-test. Endothelial tube formation, number of tubes was shown as mean ± SEM; $n = 3$ independent experiments, two-tailed Student's t-test. *$p < 0.05$, **$p < 0.01$, and ***$p < 0.001$, NS: no statistical significance.
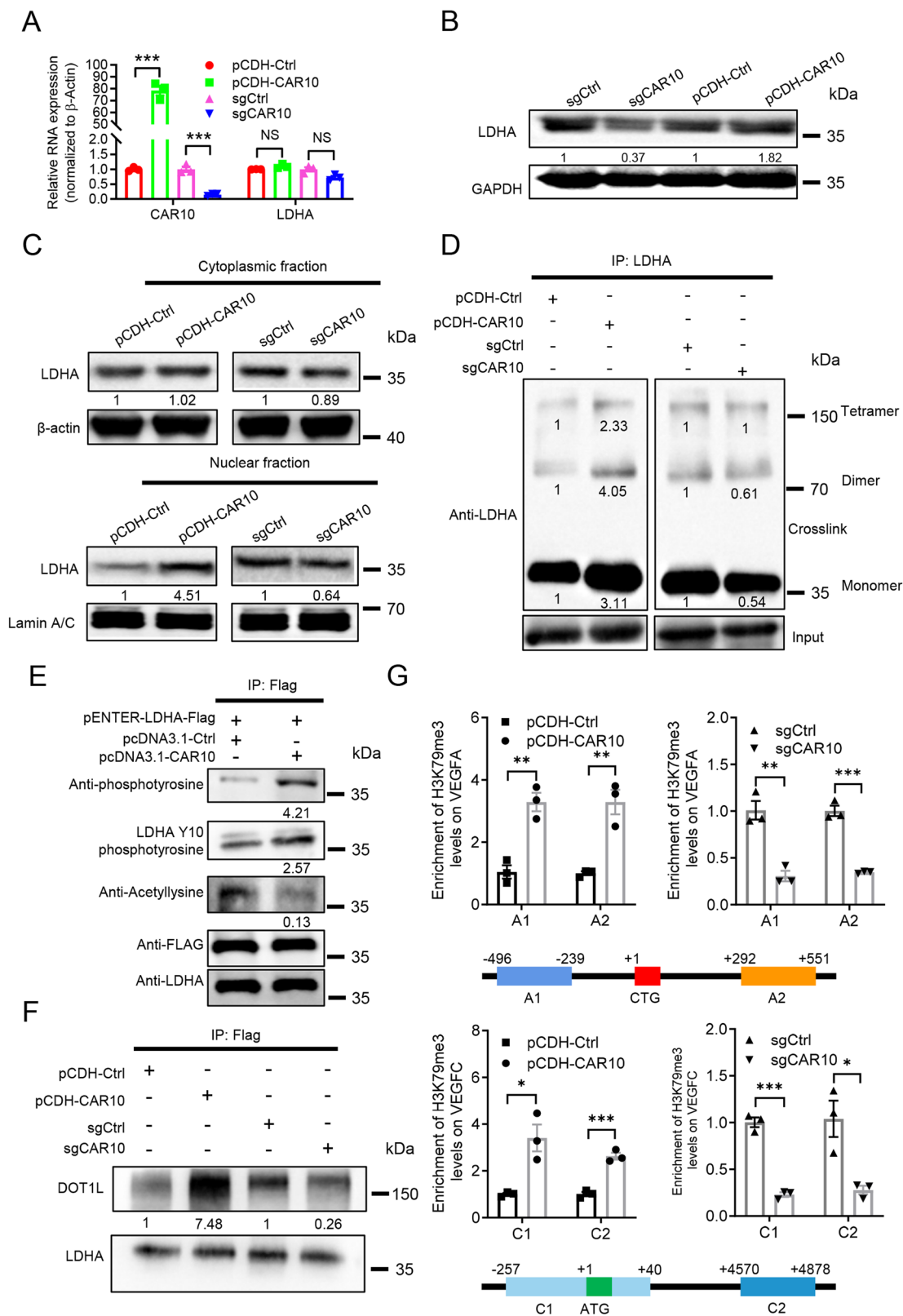
receptors to regulate both angiogenesis and lymphangiogenesis[46,47]. CAR10 could raise the expression of both VEGFA and VEGFC. In a way, CAR10 may affect the lymphangiogenesis in LUAD. However, the activity of CAR10 regulating lymphangiogenesis needs to be studied in the future.

LDHA is an important enzyme for anaerobic glycolysis and gluconeogenesis[48]. It has been widely reported that LDHA is abnormally

expressed in a variety of tumors and promotes tumor aerobic glycolysis[49]. CAR10 did not affect the mRNA level of LDHA but increased the level of LDHA protein by regulating the post-translational modification of the LDHA protein. The post-translational modification of the LDHA protein is closely related to the stability and function of the protein[44,50]. The common LDHA phosphorylation modification sites are four tyrosine

Fig. 4 | CAR10 mediates VEGFA/C epigenetic modification through regulating LDHA post-translational modification. A Expression of LDHA mRNA was detected in stably CAR10 overexpressing or knockout A549 cells. Data are presented as the mean ± SEM of three independent experiments, two-tailed Student's t-test. **B** Western blot analysis of the LDHA protein expression in A549 cells with overexpressing or knockout of CAR10. **C** Cytoplasm and nucleus fractions of stably CAR10 overexpressing or knockout A549 cells were isolated to detect LDHA expression. **D** Lysates of stably overexpressing or knockout CAR10 A549 cells were cross-linked by 0.025 % glutaraldehyde and analyzed by western blotting using LDHA antibody to examine monomer, dimer, and tetramer of LDHA. **E** Phosphorylation and acetylation of LDHA in HEK293 cells with or without overexpressing CAR10. Phosphorylated and acetylated LDHA were immunoprecipitated from cell lysates with an anti-Flag antibody, and the immunoprecipitates were analyzed by western blot using anti-phosphotyrosine, anti-LDHA Y10 phosphotyrosine and anti-acetyllysine. **F** Co-immunoprecipitation of DOT1L and LDHA in stably overexpressing or knockout CAR10 A549 cells transfected with pENTER-LDHA-Flag, followed by immunoblotting with LDHA and DOT1L. **G** ChIP-qPCR analysis was performed to study the enrichment of H3K79me3 on the promoter and the actively transcribed region of VEGFA and VEGFC. A1 (−496 to −239) corresponds to the H3K79me3 consensus sequence of VEGFA; C1 (−257 to +40) corresponds to the H3K79me3 consensus sequence of VEGFC; A2 (+292 to +551) corresponds to the actively transcribed region of VEGFA; C2 (+4570 to +4878) correspond to the actively transcribed region of VEGFC. Data are presented as the mean ± SEM of three independent experiments, two-tailed Student's t-test.*$p < 0.05$, **$p < 0.01$, and ***$p < 0.001$, NS: no statistical significance.

phosphorylation sites, including Y10, Y83, Y172, and Y239, of which Y10 phosphorylation is more common in various tumor cell lines[51]. We found that CAR10 stabilized LDHA protein expression and enhanced enzyme activity though increasing the phosphorylation of LDHA, especially LDHA Y10 phosphorylation by enhancing the interaction between LDHA and HER2/SRC, and inhibiting the acetylation of LDHA. LDHA Y10 phosphorylation enhances its activity by tetramer formation by enhancing cofactor NADH binding[51]. We observed that LDHA level in the nucleus significantly increased and more nuclear LDHA co-localized with CAR10 after CAR10 overexpression, accompanied with LDHA multimerization. Moreover, we speculate that CAR10 promoted the accumulation of Y10 phosphorylation LDHA to stimulate multimerization and nuclear translocation of LDHA. However, we didn't find CAR10 bound with multimeric LDHA because of lacking exact results, suggesting whether CAR10 facilitated nuclear translocation of dimeric LDHA by binding with dimeric LDHA or just increasing Y10 phosphorylation of LDHA.

Histone modification plays a vital role as a key epigenetic factor in the regulation of gene expression. It not only participates in many basic biological processes, but also is involved in the occurrence and development of tumors[52–54]. It has been reported in the literature[28] that nuclear LDHA increases the trimethylation level of H3K79. H3K79 methylation modification can maintain the open state of chromatin which promotes gene transcription and regulates various signal pathways[55]. We found obvious H3K79me2 modifications in the VEGFA/VEGFC gene interval (Figs. 4G and S5A–C, E). DOT1L is the only identified histone methyltransferase that catalyzes H3K79me1/H3K79me2/H3K79me3[56]. CAR10 enhanced the combination of nuclear LDHA and DOT1L to promote methylation of H3K79 in the VEGFA/C gene interval, thereby promoting the transcription and secretion of VEGFA/C. However, how CAR10 regulated the interaction between LDHA and DOT1L and positioned DOT1L to VEGFA/VEGFC gene interval remains unknown, which is worth further investigation.

The high require of oxygen for tumor growth creates a hypoxic microenvironment in majority of tumors. Hypoxic tumor microenvironment is associated with angiogenesis, tumor immune response, cell metabolism, and proliferation[57,58]. In hypoxic tumor, HIFs overexpression promotes cell proliferation by regulating MYC and TP53[59–61]. Notably, the upregulation of CAR10 inducing the angiogenesis was regulated by MYC and TP53 in LUAD (Fig. 6).

In summary, we found that CAR10 promoted angiogenesis via enhancing VEGFA and VEGFC expression. The combination of CAR10 and LDHA in cells mediated the post-translational modification, multimeric transition, and nuclear translocation of LDHA. In the cell nucleus, CAR10 promotes the combination of LDHA and DOT1L to increase the methylation of H3K79 in the VEGFA/C gene interval, thereby increasing the expression of VEGFA/C and promoting angiogenesis in LUAD tissue. The expression of CAR10 in LUAD cells was positively and negatively regulated by transcriptional profile of MYC and TP53, respectively. Cases with high expression of both CAR10 and either of LDHA/VEGFA/VEGFC tended to have the worst prognosis in comparison with the other groups. These results indicate that the CAR10-LDHA-VEGFA/C axis is a potential therapeutic and prognostic target for LUAD (Fig. S7).

Materials and methods
Mice
Female NOD-SCID mice were given from Pro. Jia Deshui, member of Shanghai General hospital affiliated with Shanghai Jiao Tong University School of Medicine. All mice were kept and bred in pathogen-free cages and provided with standard rodent chow and sterile water ad libitum at the laboratory animal center of Shanghai General hospital. All animal experimental procedures were performed in accordance with a protocol approved by the Institutional Animal Care and Use Committee of Shanghai General hospital affiliated with Shanghai Jiao Tong University School of Medicine (2019-A012-01).

Clinical specimens
Four sets of LUAD samples were collected to analyze the expression of CAR10 in para-carcinoma tissues, matched tumor tissue samples, and metastatic tissue samples. These four pairs of samples were collected from diagnosed LUAD patients with LN metastasis or other distant metastasis at the Second Xiangya Hospital (Changsha, China). The patients were informed regarding the sample collection and the patients provided informed consent by signing consent forms. Collection and use of tissue samples were approved by the Ethical Review Committee of Hunan Province Tumor Hospital and the Second Xiangya Hospital. We confirm that our study is compliant with the "Guidance of the Ministry of Science and Technology (MOST) for the Review and Approval of Human Genetic Resources." Clinic information was collected from patient medical records and is reported in Supplementary Table 1. All ethical regulations relevant to human research participants were followed.

Xenograft models
Female NOD-SCID mice, aged 4–5 weeks, were bred in the laboratory animal center of Shanghai General hospital, and kept in a specialized pathogen-free environment for roughly 1 week. As previously described[18], the xenograft tumors were established at first. The tumors were measured every 3 days 1–2 weeks after injection, and the growth curves were plotted for each group. The tumor volumes were estimated using the following formula: Volume = length × width^2 × 0.52. The tumor length should not exceed 15 mm. All mice were sacrificed 32 days after inoculation and tumors were isolated and photographed. In all experiments, the tumor length did not exceed 15 mm. Part of the subcutaneous tumors were fixed in 10% formalin and embedded in paraffin for IHC. We have complied with all relevant ethical regulations for animal use.

Cell culture
The human LUAD cell lines A549 and PC9, and HUVECs were cultured in RPMI 1640 medium (Gibco Life Technologies, Carlsbad, California, USA) and added 10% fetal bovine serum (FBS). The stable sgCAR10
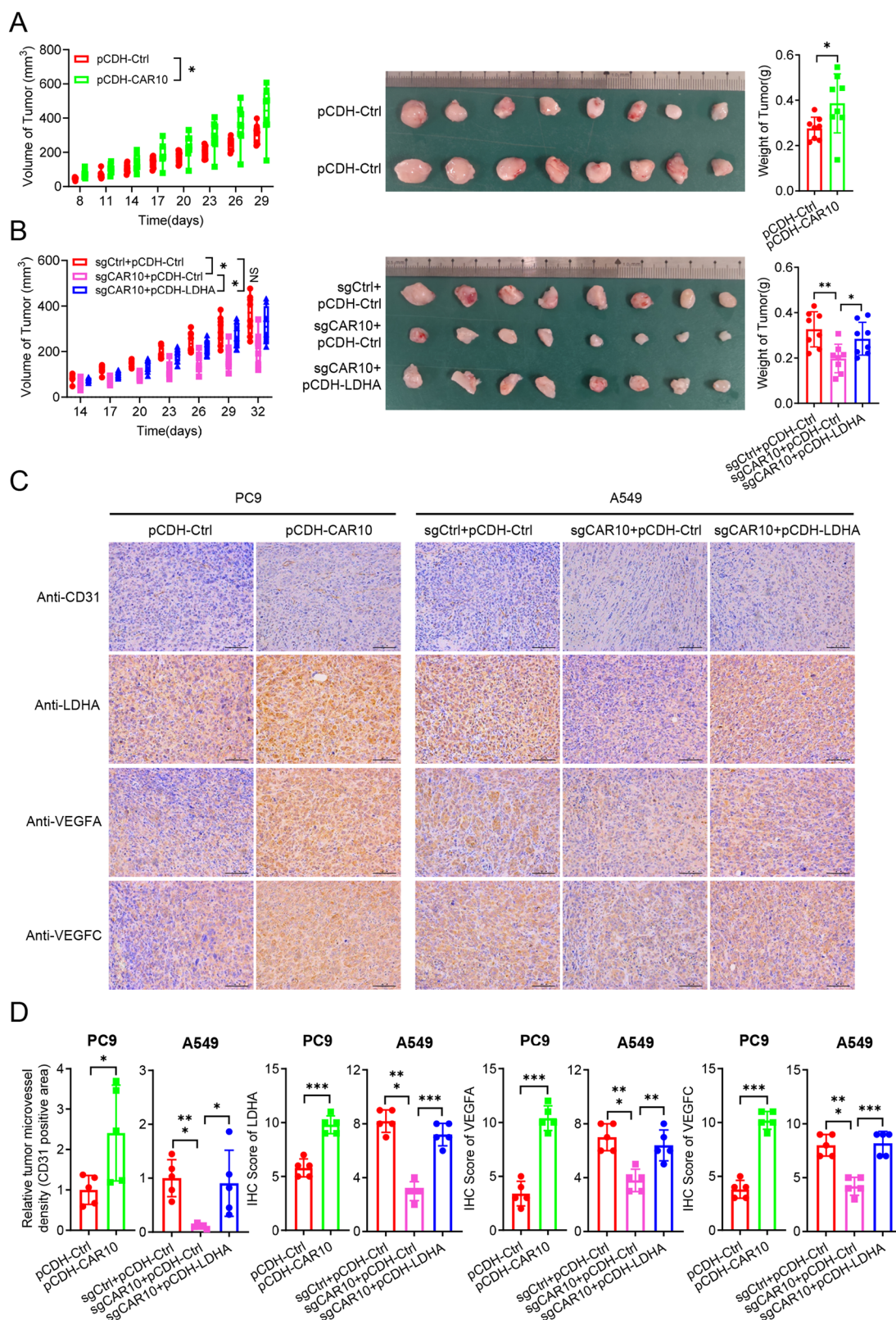
Fig. 5 | CAR10 promotes LUAD development via LDHA-VEGFA/C axis. A The overexpression of CAR10 increased the growth of PC9 cells subcutaneously transplanted xenograft into NOD-SCID mice. Data are shown as mean ± SEM; $n = 8$, two-tailed Student's t-test. Overall tumor growth of the xenografts, and tumor weights were recorded. **B** The knockout of CAR10 decreased the growth of A549 cells subcutaneously transplanted xenograft into NOD-SCID mice. However, the growth inhibition of A549 cells subcutaneously transplanted xenograft was reversed by co-overexpression of LDHA. Data are shown as mean ± SEM; $n = 8$, two-tailed Student's t-test. Overall tumor growth of the xenografts, and tumor weights were recorded. **C** IHC staining assay was performed to detect expressions of CD31, LDHA, VEGFA, and VEGFC in 7 groups mice subcutaneous xenograft tumors tissues from (A, B) (scale bar, 100 μm). **D** The proportion of relative positive signals in each group was shown as mean ± SEM ($n = 6$), using two-tailed Student's t-test. $*p < 0.05$, $**p < 0.01$, and $***p < 0.001$, NS: no statistical significance.

Fig. 6 | MYC and TP53 competitively regulated the expression of CAR10 in LUAD cells. A Schematic illustrations showing the predicted locations of TP53/MYC-binding sites in CAR10 promoter and the amplified regions of PCR for ChIP assays. **B** ChIP-PCR analysis to determine that TP53/MYC interacts with CAR10 promoter. **C** qRT-PCR was performed to detect expression of CAR10 in A549 cells transiently overexpressing or silencing TP53/MYC. Data are presented as the mean ± SEM of three independent experiments, two-tailed Student's *t*-test. **D, E** Luciferase activity of pRL-TK-CAR10 in HEK293T cells after co-transfection respectively with pCMV-TP53/siTP53/pCMV-MYC/siMYC. Data are presented as the relative ratio of firefly luciferase activity to Renilla luciferase activity. Data are presented as the mean ± SEM of three independent experiments, two-tailed Student's *t*-test. *$p < 0.05$, **$p < 0.01$, and ***$p < 0.001$, NS: no statistical significance.
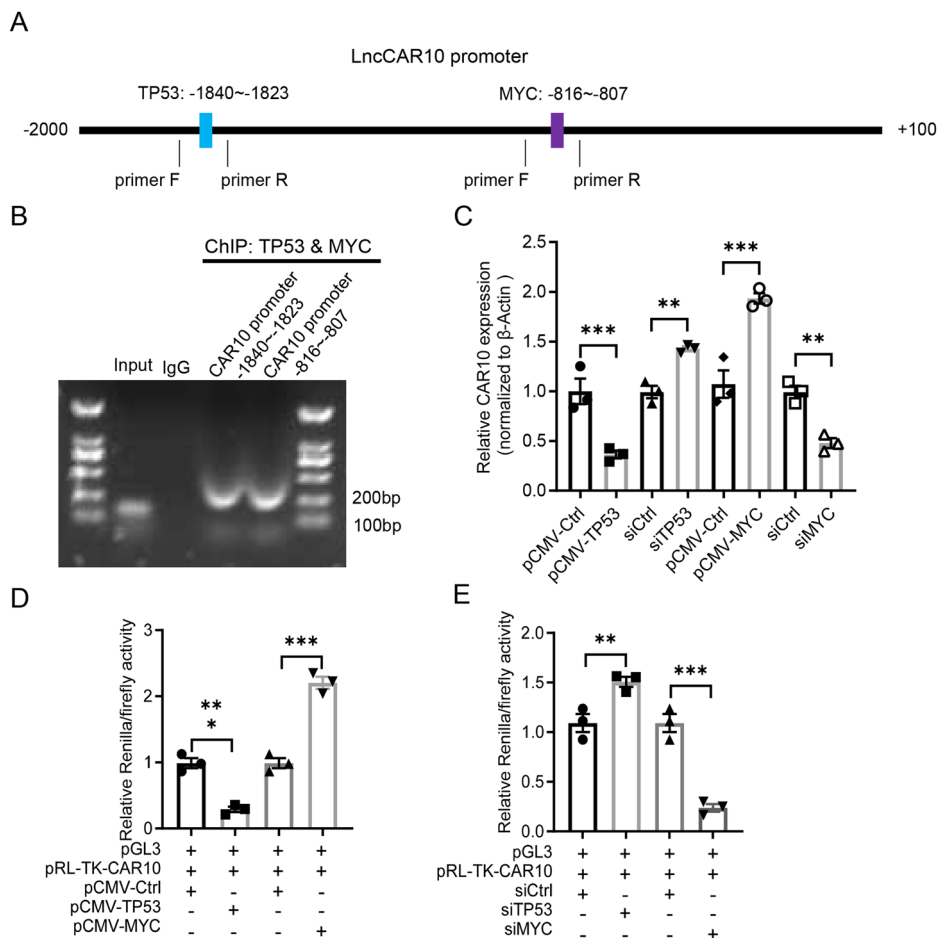
A549, sgCtrl A549, pCDH-CAR10 A549, pCDH-Ctrl A549, sgCAR10 pCDH-LDHA A549, pCDH-CAR10 PC9, and pCDH-Ctrl PC9 cells[18] were constructed by our library and cultured in RPMI 1640 medium added 10% FBS. HEK293 and HEK293T cells were cultured in Dulbecco's modified Eagle's medium (DMEM) (Gibco Life Technologies, Carlsbad, California, USA) with 10% FBS. Cells were cultured in a humidified incubator at 37 °C and under 5% CO_2. The cells were collected from the Cancer research institute, Central South University (Changsha, Hunan, China).

Plasmids, siRNAs, and cell transfection
Flag-LDHA vector was constructed based on pENTER plasmid; HIF1A, TP53, and MYC vector was constructed based on pCMV plasmid. For LDHA, TP53, and MYC knockdown, siRNAs were designed and synthesized by Sangon (Shanghai, China). The siRNAs sequences are shown in Supplementary Table 3. The plasmids were transfected into cells using Lipofectamine 3000 reagent (Invitrogen, USA).

Immunohistochemical staining
Tumor tissues were deparaffinized in xylene and hydrated in alcohol and antigens retrieved using 0.01 mM citrate buffer, pH 6.0 (Servicebio), at 100 °C for 20 min. Endogenous peroxidases were blocked by incubation of tissue slides in 3% hydrogen peroxide for 15 min at RT. 3% BSA (TBS solution) for blockage of nonspecific binding was used for anti-CD31, anti-LDHA, anti-VEGFA, and anti-VEGFC antibodies staining for 12 h at 4 °C. Then sections were incubated with a secondary HRP-labeled antibody for 2 h at RT and stained with DAB and counterstained with hematoxylin, dehydrated, and mounted. Stained sections were visualized using a microscope (Olympus, Japan).

RNA isolation and qRT-PCR analysis
TRIzol reagent (CWIO, Beijing, China) was used to extract total RNA. Nanodrop ND-2000 spectrophotometer (Thermo Scientific™, USA) was used to evaluate RNA quantity and quality. According to the manufacturer's protocol, RNA (2 μg) was reverse-transcribed into cDNA using the RevertAid First Strand cDNA Synthesis Kit (Thermo Scientific™, USA). 2 × SYBR Green qPCR Master Mix (Bimake, Texas, USA) was used to perform qRT-PCR. β-actin or GAPDH was used as an endogenous control. Relative gene expression levels were calculated via the $2^{-\Delta\Delta Ct}$ method. qRT-PCR primers of genes were synthesized by Tsingke (Beijing, China), and sequences of primers are shown in Supplementary Table 3.

Western blot (WB) analysis
Cells were extracted using radioimmunoprecipitation assay buffer (Beyotime Biotechnology, China). Sodium dodecyl sulfate-polyacrylamide gel (10%) electrophoresis was performed to separate protein (30 μg), and then protein was transferred to a polyvinylidene fluoride membrane (Millipore). After blocking with 5% nonfat milk for 1 h at room temperature, polyvinylidene fluoride membranes were incubated with specific primary antibodies in 5% bovine albumin (BSA) overnight at 4 °C. After washing three times with TBST, membranes were incubated with horseradish peroxidase-labeled secondary antibody for 1 h at 37 °C. Signals were detected using an ECL detection reagent (Bio-Rad, Hercules, CA, USA). The antibodies are listed in Supplementary Table 3.

Biotinylated RNA pull-down assay
The entire process of the experiment was carried out without ribonuclease. CAR10 and CAR10-antisense were transcribed from pcDNA3.1 CAR10 and pcDNA3.1 CAR10-antisense vectors in vitro. According to the

manufacturer's instructions, CAR10 and CAR10-antisense were treated with biotin RNA labeling mixture (Roche, Mannheim, Germany), T7 RNA polymerase (Roche), and RNase-free DNase I (Japanese, Takara). Biotin-labeled RNA was purified using an RNeasy Mini Kit (Qiagen, Germany). The lysates of A549 cells (~1×10^7) were incubated with 2 µg of purified biotin-labeled transcripts at 25 °C for 1 h, and biotin-labeled RNA was separated using Dynabeads M-270 Streptavidin (Invitrogen, USA). The proteins bound to the RNA were analyzed using liquid chromatography-mass spectrometry.

Liquid chromatography-mass spectrometry (LC-MS/MS)
The proteins bound to the CAR10 were analyzed by RNA pull-down. The production was subjected to SDS-PAGE electrophoresis and then Gels were silver-stained (Bio-Rad Silver Stain Plus, USA) by the manufacturer's instructions. Specific band was selected and enzymatically digested overnight using Sequencing Grade Modified Trypsin (cat. no. V5111, Promega, USA). After digestion, the enzymatic peptides were subjected to desalting using a C18 column and vacuum-dried and treated with 0.1% trifluoroacetic acid. The enzymatic peptides were analyzed through LTQ Orbitrap Velos Pro mass spectrometer (Thermo Scientific, Bremen, Germany) and Ultimate 3000 RSLC Nano System (Dionex, CA, USA), driven by Proteome Discoverer 1.4 software (Thermo Fisher Scientific, MA, USA). The UniProt KB/Swiss-Prot database was used to analyze the result from Proteome Discoverer 1.4 software.

RNA immunoprecipitation (RIP) assay
The plasmids pENTER FLAG LDHA, pcDNA3.1 CTR, or pcDNA3.1 CAR10 were co-transfected into HEK293T cells. After 48 h of culture, the cell lysate was obtained and incubated with Protein A and G gel beads coated with FLAG or IgG antibody overnight at 4 °C. PBS solution was used to wash protein A and G gel beads, and qRT-PCR was performed to detect CAR10 bound to FLAG-LDHA or IgG.

MS2-tagged RNA affinity purification (MS2-Trap) assay
To verify CAR10 binging with LDHA, we used the MS2-Trap assay[62]. Briefly, we cloned full-length CAR10 into pcDNA3.1(+)-MS2-12× plasmid. A549 cells were transfected with pcDNA3.1(+)-MS2-12× plasmids (control or CAR10) and MS2-FLAG-GFP plasmids. The cell lysates were immunoprecipitated using IgG, FLAG, or GFP antibodies and then detected LDHA expression by immunoblotting.

RNA fluorescent in situ hybridization (FISH)
The specific probe for LncRNA CAR10, digoxigenin-labeled, was synthesized by Sangon (Shanghai, China). A549 cells (~1×10^3) were seeded on glass coverslips in a 6-well plate and grown overnight at 37 °C. Cells were fixed with 37% formaldehyde and permeabilized using 0.5% Triton X-100. Then, cells were hybridized with specific probes overnight at 37 °C with LncRNA CAR10 in hybridization buffer. The nuclei were stained using 4′,6-diamidino-2-phenylindole (DAPI, Beyotime Biotechnology, China). Finally, cells were obtained by confocal microscope (Ultra-View Vox, Perkin-Elmer, USA). The LncRNA CAR10 probe used is listed in Supplementary Table 4.

Immunofluorescence (IF)
The cells were fixed with 37% formaldehyde and cross-linked and then blocked with Goat serum blocking solution (BOSTER Biological Technology, AR1009, China). Specific antibodies were used to incubate with the cells at 4 °C overnight and the secondary antibodies, YF 488 Goat Anti-Rabbit IgG (H&L) (US EVERBRIGHT INC, China), were treated at 37 °C for 1 h. After cbeing ounterstained with DAPI for 10 min, cells were obtained under confocal microscope (Ultra-View Vox, Perkin-Elmer, USA).

Immunoprecipitation
For immunoprecipitation, the antibodies and protein A/G magnetic beads (35 µL, Bimake, Texas, USA) were incubated together at room temperature

for 2–3 h. A549 cell lysates were extracted using GLB+ lysis buffer (150 mM NaCl, 10 mM Tris-HCl pH 7.5, 0.5% Triton X-100, 10 mM EDTA pH 8.0) with protease inhibitor cocktail (Bimake, Texas, USA) and phenylmethylsulfonylfluoride (PMSF) (Beyotime Biotechnology, China). Antibody-conjugated magnetic beads were incubated with protein in lysates for 4 °C overnight. Next, the antibody-bead complexes were collected, and the precipitated proteins were detected by western blot. The primary antibodies used are listed in Supplementary Table 4.

Separation of cytoplasmic and nuclear proteins
Assays were performed using the Minute™ Cytoplasmic and Nuclear Extraction Kit (Invent Biotechnologies, USA) according to the manufacturer's instructions. The cytoplasmic protein extraction reagent was added to the cell precipitate and supplemented with PMSF, and the cell precipitate was completely suspended and dispersed. Then, cytoplasmic protein extraction was conducted using Buffer A. After high-speed centrifugation, the supernatant containing the cytoplasmic protein was extracted. Nuclear protein extraction reagent was added to the residual precipitate, and the supernatant containing the nuclear protein was extracted.

Chromatin immunoprecipitation (ChIP)
ChIP assays were performed using a ChIP Assay Kit (Beyotime Biotechnology, P2078, China) according to the manufacturer's protocol. Briefly, formaldehyde (4%) was used to fix cells at room temperature for 10 min, followed by incubating with ChIP lysis buffer including protease inhibitors on ice for 30 min. The lysate is sonicated several times briefly to break DNA into 200–400 bp fragments immunoprecipitation was performed using an IgG or H3K79me1/me2/me3 antibody and Protein A+G Agarose incubated at 4 °C for 16–20 h. Subsequently, chromatin complexes were eluted from the beads using ChIP elution buffer as described in manufacturer's instructions. ChIP DNA was purified with DNA purification columns (TIANGEN, DP213, China). qRT-PCR was performed to detect production of immunoprecipitation using appropriate primers. Primer sequences for ChIP-qPCR are listed in Supplementary Table 3.

Cell counting Kit 8 assay (CCK8)
Cells were seeded in a 96-well plate at a density of ~1000 cells/well. CCK8 solution (20 µL, 5 mg/ml) (NCM Biotech, China) was added to each well at 0, 1, 2, 3, 4, or 5-day time points to determine changes of cell viability. The optical density of each well was determined using a scanning multi-well spectrophotometer at a wavelength of 450 nm.

Transwell invasion assay
Transwell chamber (Millipore), coated with Matrigel (Corning, USA), was used to investigate the cell invasion ability. Approximately 20,000 cells/well were seeded into the top chamber and cultured in co-culture medium. RPMI 1640 medium containing 20% serum was added in the bottom chamber. Cells were then allowed to invade for 48 h. Invaded cells were fixed with 1% formaldehyde solution and stained with 0.1% crystal violet. Then the noninvasive cells and matrigel were removed by a cotton swab. Cells on the bottom of the chamber were captured and counted using a microscope (Nikon, Japan).

Tube formation assay
The tube formation assay was conducted using HUVEC cells. Firstly, HUVECs were cultured in co-culture media for 24 h. Matrigel (100 µL) was added to each well of a 48-well plate and allowed to polymerize. Thereafter, HUVECs (4×10^4 cells/well) were seeded onto a 48-well plate with matrigel, and conditioned medium derived from different expression of CAR10/LDHA groups was added for 4 h for stimulation. The HUVEC cell tube formation was quantitatively measured using Image J software.

Dual-luciferase reporter assay
Promoter sequences of CAR10 were amplified by PCR and cloned into the pRL-TK vector (Promega, USA). HEK293T cells were seeded in 24-well

plates (~1×10^5 cells per well). Luciferase reporter gene plasmids (500 ng), pCMV-TP53/ MYC (500 ng) or control plasmid, and Firefly luciferase reporter plasmid pGL3 (500 ng) were co-transfected into HEK293T cells. After 48 h, luciferase activity was measured using the Dual-Luciferase Reporter Assay System (Promega, USA). Data were normalized against the values of the firefly luciferase.

Survival and correlation analysis of GEO data

Expression profiles, survival data, and correlation analysis for prostate cancer were downloaded from the GEO dataset (https://www.ncbi.nlm.nih.gov/geo/). The correlation map is realized by correlation analysis. Pearson's and Spearman's correlation analyses, respectively, describe the correlation between quantitative variables with or without normal distribution. OS was calculated using the Kaplan–Meier method, and the results of the analysis were considered significant in a log-rank test if $p < 0.05$.

Statistics and reproducibility

Statistical analysis was performed using GraphPad Prism 8 software. Significant differences between any two groups of data were identified using Student's t-test. One-way analysis of variance was used when assessing significant differences between multiple sets of data. All data are represented as mean ± SD or mean ± SEM. Differences were considered significant at *$p < 0.05$, **$p < 0.01$, and ***$p < 0.001$, NS: no statistical significance.

Reporting summary

Further information on research design is available in the Nature Portfolio Reporting Summary linked to this article.

Data availability

GSE30219 data are available via GEO Datasets (https://www.ncbi.nlm.nih.gov/geo/). This study is compliant with the "Guidance of the Ministry of Science and Technology (MOST) for the Review and Approval of Human Genetic Resources," which requires formal approval for the export of human genetic material or data from China. The phenotypic data that support the findings of this study are available from the corresponding author upon reasonable request. The authors declare that the uncropped western blots of this study are available within the paper and the associated supplementary information files (Supplementary Figure). As raw data of the mass spectrometry-based proteomics experiments were lost due to extenuating circumstances, we could not provide access through a repository. We have provided the original export excel files of the mass spectrometry proteomics data in the supplementary information file (Supplementary Table 2). All data generated or analyzed during this study are included in this published article and its Supplementary Information files. Please contact the corresponding author for all other data requests.

References

1. Siegel, R. L. et al. Cancer statistics, 2023. *CA Cancer J. Clin.* **73**, 17–48 (2023).
2. Wu, F., Wang, L. & Zhou, C. Lung cancer in China: current and prospect. *Curr. Opin. Oncol.* **33**, 40–46 (2021).
3. Thai, A. A. et al. Lung cancer. *Lancet* **398**, 535–554 (2021).
4. Hrustanovic, G. et al. RAS-MAPK dependence underlies a rational polytherapy strategy in EML4-ALK-positive lung cancer. *Nat. Med.* **21**, 1038–1047 (2015).
5. Hallin, J. et al. Anti-tumor efficacy of a potent and selective non-covalent KRAS(G12D) inhibitor. *Nat. Med.* **28**, 2171–2182 (2022).
6. Robichaux, J. P. et al. Structure-based classification predicts drug response in EGFR-mutant NSCLC. *Nature* **597**, 732–737 (2021).
7. Izumi, H. et al. The CLIP1-LTK fusion is an oncogenic driver in non-small-cell lung cancer. *Nature* **600**, 319–323 (2021).
8. Sung, H. et al. Global Cancer Statistics 2020: GLOBOCAN estimates of incidence and mortality worldwide for 36 cancers in 185 countries. *CA Cancer J. Clin.* **71**, 209–249 (2021).
9. Hanahan, D. & Folkman, J. Patterns and emerging mechanisms of the angiogenic switch during tumorigenesis. *Cell* **86**, 353–364 (1996).
10. Aronen, H. J. et al. High microvascular blood volume is associated with high glucose uptake and tumor angiogenesis in human gliomas. *Clin. Cancer Res.* **6**, 2189–2200 (2000).
11. Hanahan, D. & Weinberg, R. A. Hallmarks of cancer: the next generation. *Cell* **144**, 646–674 (2011).
12. Statello, L. et al. Gene regulation by long non-coding RNAs and its biological functions. *Nat. Rev. Mol. Cell Biol.* **22**, 96–118 (2021).
13. Peng, W. X., Koirala, P. & Mo, Y. Y. LncRNA-mediated regulation of cell signaling in cancer. *Oncogene* **36**, 5661–5667 (2017).
14. Liu, C. G. et al. Long non-coding RNAs and circular RNAs in tumor angiogenesis: from mechanisms to clinical significance. *Mol. Ther. Oncolytics* **22**, 336–354 (2021).
15. Chen, J. et al. LINC00173.v1 promotes angiogenesis and progression of lung squamous cell carcinoma by sponging miR-511-5p to regulate VEGFA expression. *Mol. Cancer* **19**, 98 (2020).
16. Castellano, J. J. et al. LincRNA-p21 impacts prognosis in resected non-small cell lung cancer patients through angiogenesis regulation. *J. Thorac. Oncol.* **11**, 2173–2182 (2016).
17. Mondal, T. et al. Characterization of the RNA content of chromatin. *Genome Res.* **20**, 899–907 (2010).
18. Ge, X. et al. Long noncoding RNA CAR10 promotes lung adenocarcinoma metastasis via miR-203/30/SNAI axis. *Oncogene* **38**, 3061–3076 (2019).
19. Rousseaux, S. et al. Ectopic activation of germline and placental genes identifies aggressive metastasis-prone lung cancers. *Sci. Transl. Med.* **5**, 186ra66 (2013).
20. Albini, A. et al. Cancer prevention by targeting angiogenesis. *Nat. Rev. Clin. Oncol.* **9**, 498–509 (2012).
21. Ferrara, N., Gerber, H. P. & LeCouter, J. The biology of VEGF and its receptors. *Nat. Med.* **9**, 669–676 (2003).
22. Senger, D. R. et al. Tumor cells secrete a vascular permeability factor that promotes accumulation of ascites fluid. *Science* **219**, 983–985 (1983).
23. Azoitei, N. et al. PKM2 promotes tumor angiogenesis by regulating HIF-1alpha through NF-kappaB activation. *Mol. Cancer* **15**, 3 (2016).
24. Wu, X. et al. Antibiotic bedaquiline effectively targets growth, survival and tumor angiogenesis of lung cancer through suppressing energy metabolism. *Biochem. Biophys. Res. Commun.* **495**, 267–272 (2018).
25. Deng, F. et al. Tumor-secreted dickkopf2 accelerates aerobic glycolysis and promotes angiogenesis in colorectal cancer. *Theranostics* **9**, 1001–1014 (2019).
26. Duan, X. et al. Photothermal-starvation therapy nanomodulator capable of inhibiting colorectal cancer recurrence and metastasis by energy metabolism reduction. *Adv. Healthc. Mater.* **12**, e2300968 (2023).
27. You, M. et al. Signaling pathways in cancer metabolism: mechanisms and therapeutic targets. *Signal Transduct. Target Ther.* **8**, 196 (2023).
28. Liu, Y. et al. Nuclear lactate dehydrogenase A senses ROS to produce alpha-hydroxybutyrate for HPV-induced cervical tumor growth. *Nat. Commun.* **9**, 4429 (2018).
29. Ji, Y. et al. Adenylate kinase hCINAP determines self-renewal of colorectal cancer stem cells by facilitating LDHA phosphorylation. *Nat. Commun.* **8**, 15308 (2017).
30. Guan, K. L. & Xiong, Y. Regulation of intermediary metabolism by protein acetylation. *Trends Biochem. Sci.* **36**, 108–116 (2011).

31. Jin, L. et al. Phosphorylation-mediated activation of LDHA promotes cancer cell invasion and tumour metastasis. *Oncogene* **36**, 3797–3806 (2017).

32. Steger, D. J. et al. DOT1L/KMT4 recruitment and H3K79 methylation are ubiquitously coupled with gene transcription in mammalian cells. *Mol. Cell. Biol.* **28**, 2825–2839 (2008).

33. Nguyen, A. T. & Zhang, Y. The diverse functions of Dot1 and H3K79 methylation. *Genes Dev.* **25**, 1345–1358 (2011).

34. Sun, C. et al. Tumor angiogenesis and bone metastasis—correlation in invasive breast carcinoma. *J. Immunol. Methods* **452**, 46–52 (2018).

35. Shroff, G. S. et al. Staging Lung Cancer: Metastasis. *Radio. Clin. North Am.* **56**, 411–418 (2018).

36. Popper, H. H. Progression and metastasis of lung cancer. *Cancer Metastasis Rev.* **35**, 75–91 (2016).

37. Altorki, N. K. et al. The lung microenvironment: an important regulator of tumour growth and metastasis. *Nat. Rev. Cancer* **19**, 9–31 (2019).

38. Menju, T. & Date, H. Lung cancer and epithelial-mesenchymal transition. *Gen. Thorac. Cardiovasc. Surg.* **69**, 781–789 (2021).

39. Liu, P. et al. Lymphangiogenesis in gastric cancer: function and mechanism. *Eur. J. Med. Res.* **28**, 405 (2023).

40. Ji, R. C. Hypoxia and lymphangiogenesis in tumor microenvironment and metastasis. *Cancer Lett.* **346**, 6–16 (2014).

41. Hellmann, K. Angiogenesis–time to review progress. *EXS* **61**, 26–28 (1992).

42. Halalau, F., Ghyka, G. & Haraga, L. The role of tumor angiogenesis factor (TAF) in the tumor growth. Pathological aspects. *Rom. J. Morphol. Embryol.* **36**, 189–192 (1990).

43. Wang, X. et al. A novel LncRNA HITT forms a regulatory loop with HIF-1alpha to modulate angiogenesis and tumor growth. *Cell Death Differ.* **27**, 1431–1446 (2020).

44. Niu, Y. et al. HIF2-induced long noncoding RNA RAB11B-AS1 promotes hypoxia-mediated angiogenesis and breast cancer metastasis. *Cancer Res.* **80**, 964–975 (2020).

45. Melincovici, C. S. et al. Vascular endothelial growth factor (VEGF)—key factor in normal and pathological angiogenesis. *Rom. J. Morphol. Embryol.* **59**, 455–467 (2018).

46. Lim, L. et al. Hemostasis stimulates lymphangiogenesis through release and activation of VEGFC. *Blood* **134**, 1764–1775 (2019).

47. Chaudary, N., Milosevic, M. & Hill, R. P. Suppression of vascular endothelial growth factor receptor 3 (VEGFR3) and vascular endothelial growth factor C (VEGFC) inhibits hypoxia-induced lymph node metastases in cervix cancer. *Gynecol. Oncol.* **123**, 393–400 (2011).

48. Yang-Feng, T. L. et al. Localization of the LDHA gene to 11p14—11p15 by in situ hybridization of an LDHA cDNA probe to two translocations with breakpoints in 11p13. *Hum. Genet.* **74**, 331–334 (1986).

49. Hou, X. et al. LDHA induces EMT gene transcription and regulates autophagy to promote the metastasis and tumorigenesis of papillary thyroid carcinoma. *Cell Death Dis.* **12**, 347 (2021).

50. Wang, W. T. et al. The lncRNA LAMP5-AS1 drives leukemia cell stemness by directly modulating DOT1L methyltransferase activity in MLL leukemia. *J. Hematol. Oncol.* **13**, 78 (2020).

51. Fan, J. et al. Tyrosine phosphorylation of lactate dehydrogenase A is important for NADH/NAD(+) redox homeostasis in cancer cells. *Mol. Cell. Biol.* **31**, 4938–4950 (2011).

52. Bajbouj, K. et al. Histone modification in NSCLC: molecular mechanisms and therapeutic targets. *Int. J. Mol. Sci.* **22**, 11701 (2021).

53. Wang, R. et al. The functions of histone modification enzymes in cancer. *Curr. Protein Pept. Sci.* **17**, 438–445 (2016).

54. Hanahan, D. Hallmarks of cancer: new dimensions. *Cancer Discov.* **12**, 31–46 (2022).

55. Farooq, Z. et al. The many faces of histone H3K79 methylation. *Mutat. Res. Rev. Mutat. Res.* **768**, 46–52 (2016).

56. Wood, K., Tellier, M. & Murphy, S. DOT1L and H3K79 methylation in transcription and genomic stability. *Biomolecules* **8**, 11 (2018).

57. Wicks, E. E. & Semenza, G. L. Hypoxia-inducible factors: cancer progression and clinical translation. *J. Clin. Investig.* **132**, e159839 (2022).

58. Brahimi-Horn, M. C., Chiche, J. & Pouyssegur, J. Hypoxia and cancer. *J. Mol. Med.* **85**, 1301–1307 (2007).

59. Greijer, A. E. & van der Wall, E. The role of hypoxia inducible factor 1 (HIF-1) in hypoxia induced apoptosis. *J. Clin. Pathol.* **57**, 1009–1014 (2004).

60. Bhandari, V. et al. Divergent mutational processes distinguish hypoxic and normoxic tumours. *Nat. Commun.* **11**, 737 (2020).

61. Malchenko, S. et al. Stabilization of HIF-1alpha and HIF-2alpha, up-regulation of MYCC and accumulation of stabilized p53 constitute hallmarks of CNS-PNET animal model. *PLoS ONE* **12**, e0173106 (2017).

62. Yoon, J. H., Srikantan, S. & Gorospe, M. MS2-TRAP (MS2-tagged RNA affinity purification): tagging RNA to identify associated miRNAs. *Methods* **58**, 81–87 (2012).

Acknowledgements

Author contributions

Z.L. designed the study. X.L.G. and C.D. completed major experiments and wrote the manuscript. Z.Y.W. interpreted the data and performed the statistical analysis. W.X. performed some of the experiments. J.H.L. and L.F. contributed to the sample collection. M.Z. and J.J.X. revised the manuscript. Z.L. and Y.J.C. are responsible for research supervision and funding acquisition. All authors read and approved the final manuscript.

Competing interests

The authors declare no competing interests.

Additional information

Supplementary information The online version contains supplementary material available at https://doi.org/10.1038/s42003-025-07452-x.

Correspondence and requests for materials should be addressed to Ziyao Wang or Zheng Li.

Peer review information *Communications Biology* thanks the anonymous reviewers for their contribution to the peer review of this work. Primary Handling Editor: Johannes Stortz. A peer review file is available.

Reprints and permissions information is available at http://www.nature.com/reprints

Publisher's note Springer Nature remains neutral with regard to jurisdictional claims in published maps and institutional affiliations.